Journal of Materials Chemistry A

Expanding the Potential of Redox Carriers for Flow Battery Applications

Journal:	*Journal of Materials Chemistry A*
Manuscript ID	TA-ART-04-2020-004511.R2
Article Type:	Paper
Date Submitted by the Author:	06-Aug-2020
Complete List of Authors:	Andrade, Gabriel; Los Alamos National Security, LLC., MPA Materials Synthesis and Integrated Devices Popov, Ivan A.; Los Alamos National Laboratory, Theoretical Division T-1 Federico, Celia; Los Alamos National Security, LLC., MPA Materials Synthesis and Integrated Devices Yang, Ping; Los Alamos National Laboratory, Theoretical Division Batista, Enrique; Los Alamos National Laboratory, Theoretical Division Mukundan, Rangachary; Los Alamos National Laboratory, MPA-11 Davis, Benjamin; Los Alamos National Security, LLC., MPA Materials Synthesis and Integrated Devices

Article type: Full

Title: Expanding the Potential of Redox Carriers for Flow Battery Applications

Author(s), and Corresponding Author(s)*,‡ Andrade, Gabriel A. ‡; Popov, Ivan. A.‡; Federico, Celia R.; Yang, Ping*; Batista, Enrique R.*; Mukundan, Rangachary; Davis, Benjamin L.*

Dr. G. A. Andrade, Celia R. Federico, Dr. R. Mukundan, Dr. B. L. Davis
MS K763
MPA-11: Materials Synthesis and Integrated Devices
Los Alamos National Laboratory
Los Alamos, New Mexico, USA, 87544
*E-mail: bldavis@lanl.gov

Dr. I. A. Popov, Dr. P. Yang
MS B221
T-1: Physics and Chemistry of Materials
Los Alamos National Laboratory
Los Alamos, New Mexico, USA, 87544
*E-mail: pyang@lanl.gov

Dr. E. R. Batista
MS B258
T-CNLS: Center for Nonlinear Studies
Los Alamos National Laboratory
Los Alamos, New Mexico, USA, 87544
*E-mail: erb@lanl.gov

‡These authors contributed equally.

Keywords: redox flow battery, expanded window, non-aqueous

TOC: Small synthetic changes, Big Voltage Impact

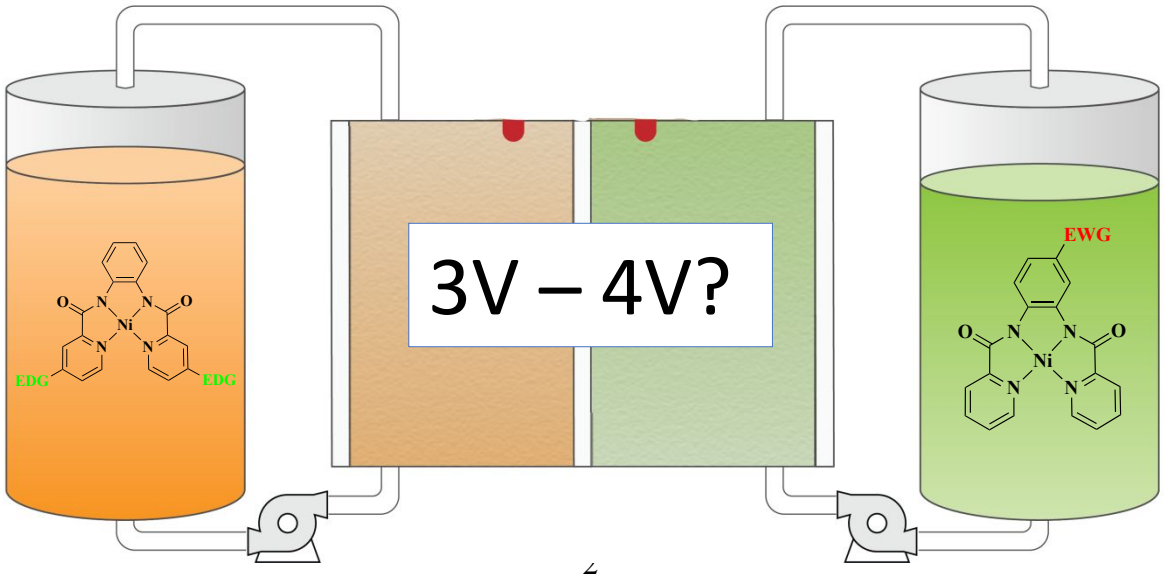

Abstract

Using theoretical modeling to guide our approach, substituents were selected to improve the negative and positive potentials associated with a representative metal-based redox carrier, a phenyl spaced nickel bispicolinamide complex, [Ni(bpb)], **1**. To broaden the cell potential, electron donating groups were selected and installed on the pyridyl moieties, [Ni(bpb-$(NMe_2)_2$)], **2**, while electron withdrawing groups were incorporated on the phenyl linker, [Ni(bpb-R)] (R = -F, $-CF_3$, and $-NO_2$), **3**-**5**. Our model predicts an increase of ~300mV and ~500mV for the first and second negative waves of Ni(bpb-NMe_2), **2**, and up to ~330mV and ~210 mV increase to the first and second positive waves in **3**-**5**. The modeled complexes were synthesized in good yields using a modification of the literature procedure. Due to limited solubility, the differential pulse voltammetry was measured on complexes **2**-**5** using a drop cast technique. Comparison of the observed and predicted potentials is discussed in acetonitrile (MeCN) and dimethylformamide (DMF) solvents.

Introduction

In the continuing quest to find new ways to store renewable energy that interface with our ever-growing demand, we focused our acumen on nonaqueous redox flow batteries (RFB). RFBs stand apart from traditional batteries, where the electrode sets the limit of stored capacity, by using molecular or oligomeric/polymeric redox carriers stored outside the cell.[1–5] Thus, in a non-hybrid forms, power (cell stack) and energy (tanks) are fully decoupled and allow for flexible end-user implementations. Of course, such promise has hefty demands – the redox carriers are asked to perform at extreme potentials, form concentrated solutions (> 1M) that aren't too viscous, not embark on irreversible side reactions, and do this over a 20-year lifecycle. Very few manifestations even flirt with all of these criteria,[6,7] and only a few aqueous systems have been tested that may meet these lifecycle requirements.[8] Recent work on novel electrode designs may facilitate aqueous vanadium RFBs to achieve the lifetime requirements[9] – many more hurdles are required for nonaqueous systems.[2] Indeed, solubility of active species also plays an important role for the performance of RFBs. Various strategies on solubility tuning of charge carriers have been reported elsewhere.[10,11] Other studies demonstrated an effective way to significantly improve the reaction kinetics and redox capacity[12] and computationally explored stability and reversibility of redox species for RFBs.[13]

Rather than try to find a redox carrier that meets all of these criteria, we endeavored to explore whether energy density could be improved by tuning the redox waves. This has already been examined in aqueous systems, most notably with quinones[14] demonstrating some variation in potential. In the nonaqueous realm, there have been modifications to posolytes (ferrocene,[15] cyclopropenium[16]) and negolytes (cobaltocene,[17] metal clusters[18]). Some systems, such as the polyoxovandate-alkoxide clusters,[19] can be tuned with metal and ligand substitutions, although the ligand changes only exhibit a minor impact.[18] A summary of

selected redox carrier potential changes is shown in Table 1.

	Redox Carrier	Base Potential (V)	Substitution	New Potential (Change)
Posolyte	Fc[15]	3.26 (vs. Li/Li^+) 0.3 (vs. SHE)	Fc-CH_2N^+EtMe2	3.4 (0.23)
			C_5H_4C=OMe	0.65 (0.35)
	Cyclopropenium[16]	0.83 (vs. Fc)	Thioether	1.33 (**0.5**)
Negolyte	AQDS *Aqueous*[8]	0.21 (vs. SHE)	DHAQDMS	0.02 (0.19)
	Cp_2Co[17]	-1.1 (vs. SHE)	Cp^*_2Co	-1.65 (**0.55**)
	Lindqvist POV[19] $V_6O_7(OMe)_{12}$	-0.72, -0.22 (vs. Ag^+)	Ti_2V_4	-2.1, -1.58 (**1.38, 1.36**)
Both	Lindqvist POV[18] $V_6O_7(OEt)_{12}$	0.22, 0.79 -0.88, -0.34	-NMe_3 variant	0.46, 1.00 -0.67, -0.11 (0.21-0.24)

Table 1. Redox Carriers and modified variations used in RFBs.
Bold potential changes are to highlight large magnitude changes
AQDS = anthraquinone-2,7-disulfonic acid
DHAQDMS = 1,4-dihydroxyanthraquinone-2,3-dimethylsulfonic acid
Cp = C_5H_5, Cp* = C_5Me_5, Fc = ferrocene, Cp_2Fe; POV = polyoxovanadate

In order for any RFB to be deployed on a significant scale, the cost must come down. One mechanism for that goal to be achieved is through improving the cell potential above 2V; better yet 3V and above.[20] As Table 1 indicates, changes in metal center provide the largest impact for a particular system (polyoxometalate) with functional group changes only providing modest impact of 0.2-0.5 V. Of course, if both the posolyte and negolyte can be modified readily, the cell could be improved by ~1V.

We previously reported nickel systems, which displayed promising voltammograms and cycled well through the initial negative wave.[21] While one of the complexes studied, Ni(bpb), **1**, displayed low currents due to low solubility, we found that **1** would be a good model

compound to study because it contained qualitatively reversible positive and negative waves that might be influenced with judicious incorporation of functional groups, *vide infra*. Theoretical studies of the phenyl spaced bispicolinamide nickel complex, **1**, found that the negative waves corresponded to a metal-based reduction, followed by reduction of the ligand at the pyridine ring. The addition of electron donating groups (EDG) to the pyridyl periphery should make these events more difficult to reduce, resulting in a more negative reduction potential. Similarly, the positive waves corresponded to oxidation at the metal followed by oxidation of the ligand, although at the phenyl linker. Addition of electron withdrawing groups (EWG) on the phenyl backbone should make these events harder to oxidize and thus lead to more positive oxidation waves (Eq. 1).

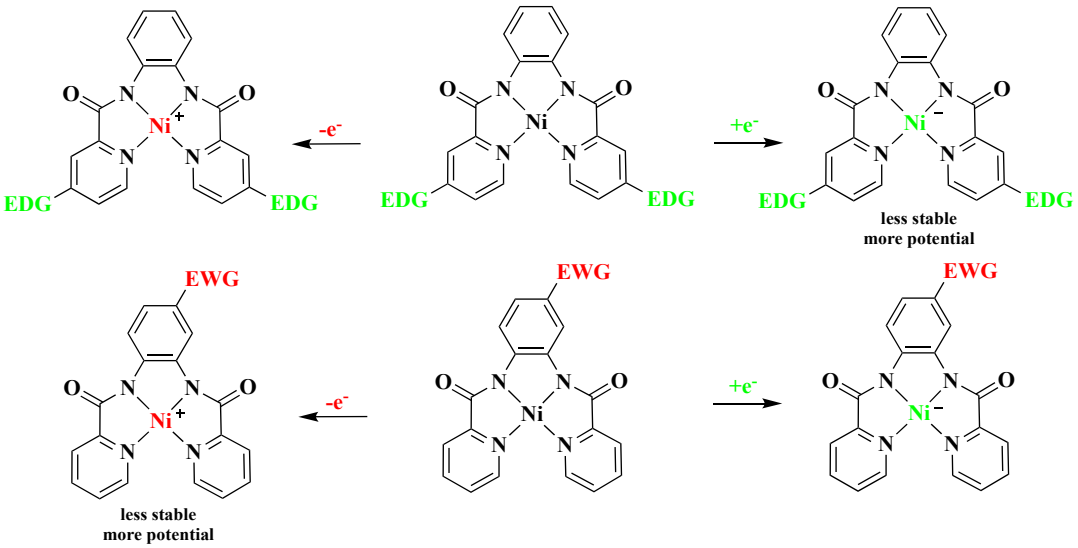

Equation 1. Generalized equations showing Ni(bpb) equipped with electron donating groups (EDGs, green, above) or electron withdrawing groups (EWGs, red, below) and the associated oxidized/reduced complexes.

Due to the simplicity in synthesis of this class of compounds, we sought commercially available starting materials to accomplish these modifications and test our hypothesis. Using theoretical guidance, and availability of starting materials, NO_2, F, and CF_3 groups were targeted as EWGs, and NMe_2 as the EDG. The synthesis of the proligands was accomplished using a common one-pot peptide coupling strategy and metalation was also easily accomplished with good overall yields. The results indicated that the target compounds were successful in altering

the redox potential of the 2nd positive and negative waves by ~0.5V.

Results and Discussion

Potential Change Predictions.

Using previously described methods,[22] complexes **1-5** were modeled to predict their redox potentials and the localization of the electron upon oxidation/reduction in DMF (Table 3) and in MeCN (Table S3). Regardless of the solvent, for complexes **2-5** with an EDG or EWG, the oxidations follow intuition with EDG making the process more facile (complex **2**) and more difficult with EWG substitutions (complexes **3**-**5**). The changes predicted in these complexes are worth highlighting specifically: an increase of ~300mV and ~500mV for the first and second negative waves of [Ni(bpb-$(NMe_2)_2$)], **2** and up to ~330mV and ~210 mV increases to the first and second positive waves in **3**-**5**, respectively. These increases, if combined in the same cell, would result in a significant increase in cell potential. Similar potential changes are found when the solvent medium is MeCN (Table S3).

Synthesis of Materials.

The synthetic pathway to prepare the phenyl bridged di-picolinamide nickel complexes is shown in Scheme 1. The preparation began with coupling of o-phenlyenediamine derivatives with picolinic acid derivatives using HATU (1-[Bis(dimethylamino)methylene]-1H-1,2,3-triazolo[4,5-b]pyridinium 3-oxide hexafluorophosphate) to generate the target diamide proligands. HATU was used as the conditions and reagents are much milder than previously reported in the literature and worked as a general method for all derivatives.[23] The respective metal complexes were generated rapidly by deprotonation of the amide protons with trimethylamine and adding nickel(II) tetrafluoroborate hexahydrate to precipitate the target complexes in high yields (79 to 95%). Using this pathway, we were able to synthesize a group

of complexes with the desired electron withdrawing and donating groups (Scheme 1), labelled as [Ni(bpb)], **1**, [Ni(bpb-$(NMe_2)_2$)], **2**, [Ni(bpb-F)], **3**, [Ni(bpb-CF_3)], **4** and [Ni(bpb-NO_2)], **5**.

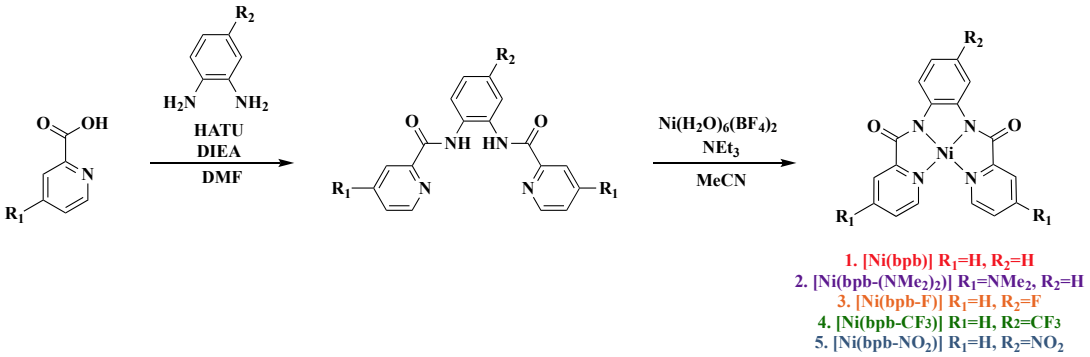

Scheme 1. Synthesis of bispicolinamide variants

Examining the IR stretch of the C=O in each complex, a predictable trend is observed of greater double bond character for stronger EWG on the phenyl linker. NO_2 has the strongest withdrawing power in complex **5**, yielding a stretch of 1653 cm^{-1}; -CF_3 is comparable with 1648 cm^{-1} in complex **4** and -F is weaker still with 1632 cm^{-1} in complex **3**. In the case of complex **2**, without any phenyl substitution, the 1604 cm^{-1} stretch indicates the most donation into the amide functionality resulting in the least double bond character. The reduced donating power of the amide nitrogen is a portent for the changes in reduction potentials (*vide infra*).

Electrochemical Analysis.

Evaluation of the electrochemical impact of substitution on **1** was initially attempted using standard cyclic voltammetric methods: acetonitrile (MeCN) solvent, hexafluorophosphate supporting electrolyte. Due to poor solubility in MeCN, several solvents were tried and DMF was found to dissolve complexes **1-4** sufficiently for CV measurement (Fig 1, Table 2). The small currents observed precluded quantitative analysis of the waves, but qualitatively a few trends are apparent. When an EDG is appended to the pyridyl moieties (complex **2**), the resulting waves associated the ligand's reduction are shifted to move negative potentials, with 2nd event at the periphery of the solvent window. Conversely, when EWGs are attached to the phenyl linker (complexes **3** and **4**), the positive waves are shifted more positive and separated

from each other. In attempt to get more confidence in our $E_{1/2}$ assignments, we explored drop casting complexes **1-5** onto the carbon electrodes. Control experiments with **1** (Fig S1 and S2) indicate excellent agreement between the $E_{1/2}$ observed by CV, validating this approach. The differential pulse voltammetry (DPV) of **1** and **2** (Fig 2a) shows the donating group -NMe_2 shift the negative waves by ~0.5V. The impact of EWGs is also now easier to visualize (Fig 2b), with both positive waves shifting 0.3-0.5V upon substitution with -CF_3 or -NO_2. The influence of -F is less clear, as the prominent positive feature is at nearly the same potential as **1** with a small feature at a slightly larger potential (~1V).

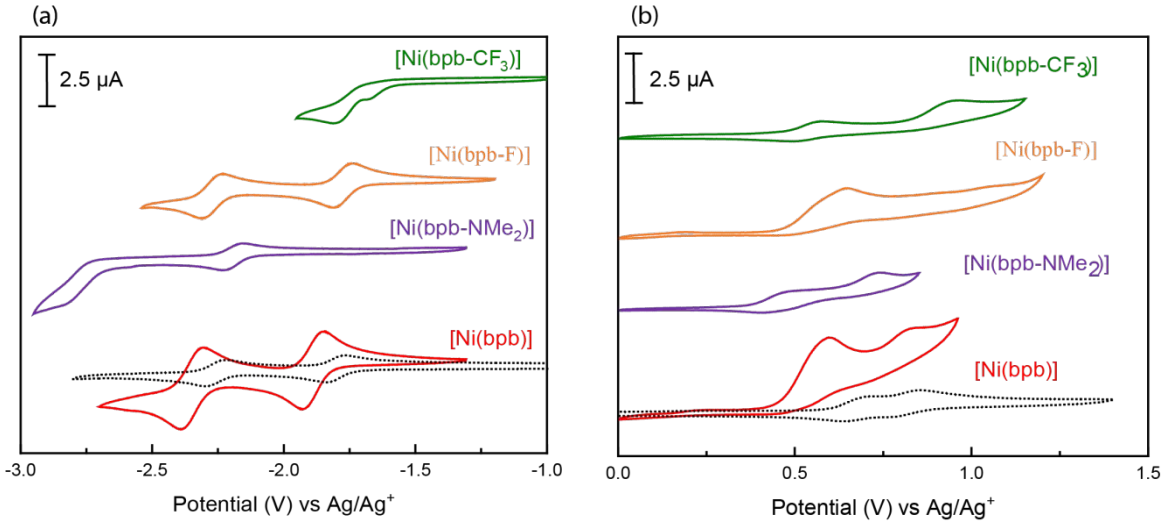

Figure 1. Voltammograms of **1** in DMF (red solid line), **1** in MeCN (black dotted line), **2** in DMF (purple), **3** in DMF (orange), and **4** in DMF (green). Data shown is obtained from 3rd sweep.

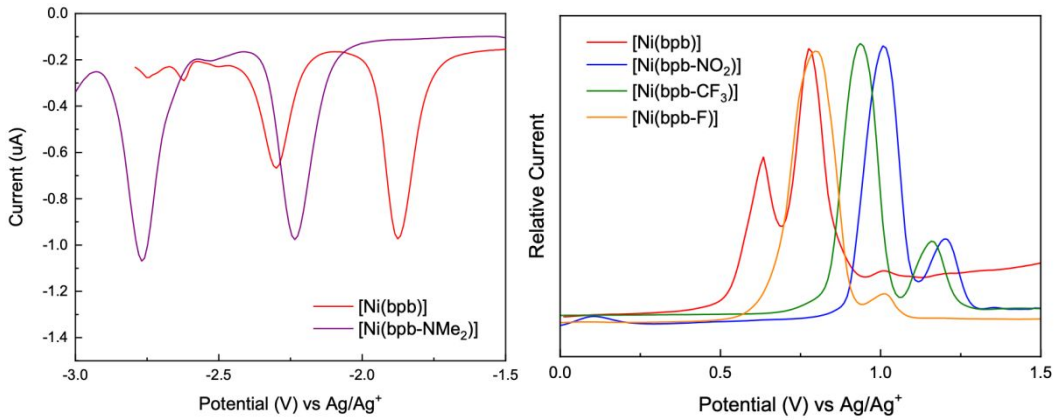

Figure 2. DPV for drop cast complexes **1** and **2** (left), and complexes **1**, **3-5** (right).

Complex	I_p 2nd Reduction (V)	I_p 1st Reduction (V)	I_p 1st Oxidation (V)	I_p 2nd Oxidation (V)
[Ni(bpb)], 1	–2.35 V	–1.96	0.55	0.68
[Ni(bpb-NMe_2)], 2	–2.86 (–0.51)	–2.33 (–0.37)	0.48 (–0.07)	0.79 (+0.11)
[Ni(bpb-F)], 3	–2.39 (–0.04)	–1.96 (0.0)	0.72 (+0.17)	0.92 (+0.24)
[Ni(bpb-CF_3)], 4	–2.35 (0.0)	–2.17 (–0.21)	0.85 (+0.30)	1.07 (+0.39)
[Ni(bpb-NO_2)], 5	–2.34 (+0.01)	–2.00 (–0.04)	0.93 (+0.38)	1.15 (+0.47)

Table 2. Summary of potentials (V) observed by DPV experiments with dropcast complexes (diff from complex **1**). Corrected to Fc as a reference (-0.087V)

To assess whether the incorporation of an EWG or EDG had a desirable impact on the electrochemical properties, we examined how the $E_{1/2}$ of the waves changed relative to each other and the spacing between the most negative/positive waves. The results (Table S1) indicate, with the exception of negative wave differences in complexes **4/5** (negative percentage changes**)**, that the spacing increased by 0.07-0.18V relative to complex **1** in nearly all cases. Additionally, the widest spacing (right most column) between the most negative/positive waves improved by 0.07-0.62V, equating to a 3-20% increase. These data show that judicious installation of an EWG or EDG substituent can improve the voltaic qualities of a redox carrier.

Comparison with the Computed Reduction Potentials

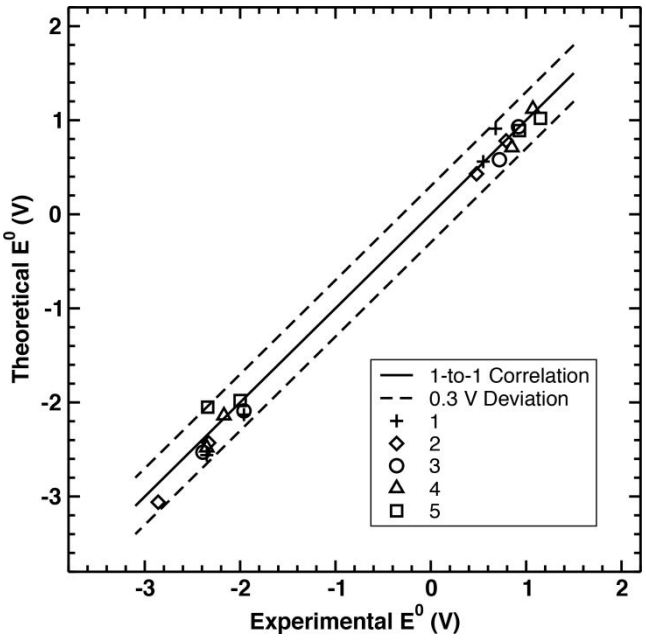

Figure 3. Computed vs. experimental reduction potentials (V) of complexes **1**-**5** in DMF in the {2+ → 2−} range of charge states. Theoretical reduction potentials corresponding to the metal-centered events are depicted in the 2+ → 1+ and 0 → 1− steps, and to the ligand-centered events in the 1+ → 0 and 1− → 2− steps.

The theoretical calculation of the redox potentials yielded insight into the nature of the redox events at each step (metal- or ligand-based reduction/oxidation) in the {2+ → 2−} range of charge states. Most of the calculated reduction potentials are found within 0.2V of the corresponding experimental values (Fig 3, Table 3), with only a few of them within 0.3V, in accordance with the error bar, previously proposed for the calculation of reduction potentials within the revised Born-Haber approximation.[22] This approach has previously been successfully applied to various Ni- and Fe-based charge carriers as described elsewhere.[21,24,25] For clarity in the following discussion, the electrochemical waves are described relative to 0V, e.g. the 'first' wave is closest to 0, followed by the second, etc. The charge state of 0 ([**1**-**5**]^0) corresponds to neutrally charged complexes (Ni^{2+}, L^{2-}), while the 1+/2+ and 1−/2− charge states correspond to their oxidized and reduced forms, respectively. Comparing the experimental and computed reduction potentials for the 1+ → 0 step, it is concluded that the

Complex/ reduction step	[Ni(bpb)], **1**		[Ni(bpb-$(NMe_2)_2$)], **2**		[Ni(bpb-F)], **3**		[Ni(bpb-CF_3)], **4**		[Ni(bpb-NO_2)], **5**	
	Exp.	Theor.	Exp.	Theor.	Exp.	Theor.	Exp.	Theor.	Exp.	Theor.
2+ → 1+	0.68	**1.05 [L]** 0.91 [M]	0.79	**0.99 [L]** 0.78 [M]	0.92	**1.06 [L]** 0.93 [M]	1.07	**1.25 [L]** 1.12 [M]	1.15	**1.38 [L]** 1.02 [M]
1+ → 0	0.55	**0.42 [M]** 0.56 [L]	0.48	**0.23 [M]** 0.43 [L]	0.72	**0.44 [M]** 0.58 [L]	0.85	**0.57 [M]** 0.71 [L]	0.93	**0.53 [M]** 0.89 [L]
0 → 1−	−1.96	**−2.13 [M]**	−2.33	**−2.43 [M]**	−1.96	**−2.09 [M]**	−2.17	**−2.14 [M]**	−2.00	**−1.98 [M]**
1− → 2−	−2.35	**−2.56 [L]**	−2.86	**−3.06 [L]**	−2.39	**−2.53 [L]**	−2.35	**−2.48 [L]**	−2.34	**−2.05 [L]**

Table 3. Redox potentials experimentally measured and modeled for the [Ni(bpb-R)] series in DMF. All potentials reported are vs. Fc and are reported as $E_{1/2}$ unless the peak is irreversible, in which case the E_p is reported. [L] or [M] indicates ligand- or metal-centered events, respectively. Theoretical values shown in bold correspond to the redox potentials based on the most thermodynamically stable electronic configurations. For the 1+ → 0 and 2+ → 1+ steps, two values of reduction potentials are shown based on the two possible localization sites in the $[Ni(bpb\text{-}R)]^{1+}$ complexes for comparison. Theoretical reduction potentials of complexes **1**-**5** obtained in MeCN are summarized in Table S3.

first oxidation of all **1**-**5** complexes in DMF should be regarded as ligand-based due to the removal of an electron from the aryl moiety and amide linker (Tables S9, S13, S17, S25). However, the first oxidation of complex **1** in MeCN solvent was previously[21] suggested to be metal-centered (Ni^{3+}) due to the analogy to the redox potentials in similar Ni(bpen) and Ni(bppn) as well as Co- and Fe-coordination complexes featuring aryl linkers. From the free energy calculations of the $[\mathbf{1}]^{1+}$ complex in DMF, removal of an electron from the metal (M^{3+}) or from the ligand (L^{1-}) is energetically indistinguishable (within the errors expected for these calculations), although slightly favoring the metal oxidation, *i.e.* by ~0.14 eV (Table S5). In MeCN, this difference is even smaller, *i.e.* 0.05-0.07 eV, but in favor of the ligand oxidation (Table S4). Hence, the assignment of where the electron comes from is equivocal for complex $[\mathbf{1}]^{1+}$. In any scenario, values of the reduction potentials for the 1+ → 0, and consequently, the 2+ → 1+ events are very similar to each other regardless of the assignment (Table 3). For the EWG- or EDG-substituted complexes $[\mathbf{2}\text{-}\mathbf{5}]^{1+}$, the energy difference between metal- and ligand-centered oxidation gets larger in DMF, in favor of the metal-based oxidation (Table S5), while the ligand-centered first oxidations are favored in MeCN based on the most

thermodynamically stable [**2**-**5**]$^{1+}$ configurations (Table S3). Comparing the experimental and computed reduction potentials in DMF for all **1**-**5** complexes, it is clear that the theoretical ligand-centered events show better agreement with the experimental data for the 1+ → 0 step (0.01-0.14 eV deviation for the ligand-centered events *vs.* 0.13-0.40 eV for the metal-centered events).

Assuming ligand-based event for the first oxidation, the 2+ → 1+ step corresponding to the second oxidation is assigned to the metal-based event resulting in Ni^{3+} species. Specifically, the 2+ state is characterized as a broken-symmetry singlet state with an unpaired electron on the metal antiferromagnetically coupled with the one on the 1,2-diaminobenzene moiety (Tables S8, S9, S12, S13, S16, S17, S20, S21, S24, S25), similar to the case of the $[Fe^{III}(bpb)^{ox1}(CN)_2]$ complex.[26] The assignment of the electron localization is in accordance with the experimental reduction potential data, demonstrating a better agreement for the metal-based second oxidation than for the ligand-based event (0.01-0.23 eV deviation for the metal-centered events *vs.* 0.14-0.37 eV for the ligand-centered events).

Similar to complex **1**, in the negative waves of complexes **2**-**5**, the first reduction places the electron on the metal (Ni^{1+}), whereas in the second reduction pyridyl moieties accept an electron antiferromagnetically coupling with the metal. Thus, it is concluded that the nature of the redox events for complexes **2**-**5** is identical to that of complex **1** in the entire range of {2+ → 2−} charge states, with the reduction potentials getting more negative for the EDG-substituted complex **2** in the negative waves, and more positive for the EWG-substituted complexes **3**-**5** in the positive waves. It is worth noting that according to our calculations the same conclusions are drawn for both DMF and MeCN solvents (Tables S3-S27). As one would expect, both solvents are redox innocent throughout the {2+ → 2−} charge states in all complexes.

It is also worthy to note that upon functionalization geometries of the EWG- or EDG-substituted complexes stay close to the original complex **1**[21] at their respective charge states, regardless of a solvent (Figs S3-S6, Tables S6, S7, S10, S11, S14, S15, S18, S19, S22, S23). While the neutral $[Ni(bpb\text{-}R)(DMF)_2]^0$ and ligand-based oxidized form, $[Ni(bpb\text{-}R)(DMF)_2]^{1+}$, of complexes **1-5** exhibit square-planar geometries (Fig S4) with weakly bound DMF molecules, forming Ni^{3+} produces complexes with two DMFs directly coordinating to Ni in axial positions ($R(Ni\text{-}O_{DMF})$=2.10-2.12 Å in all **1-5**. Similar coordination modes are found in the $[Ni(bpb\text{-}R)(MeCN)_2]^{0/1+/2+}$ complexes (Fig S3), where MeCN molecules also form the shortest bonding with the Ni center at the 2+ charge state ($R(Ni\text{-}N_{MeCN})$=2.15-2.18 Å).

Conclusion

The modification of redox carriers used in RFBs can have a profound impact on their performance metrics. For complex **2**, the change predicted for its 1st and 2nd negative waves, ~300mV and 500mV, were very close to the measured changes of 370mV and 510mV; likewise, for complexes **3-5**, predictions of up to 330mV and 210mV were also reasonable to the measured changes of 380mV and 470mV. The resulting potential changes for the posolyte are modest compared to the state of the art (cyclopropenium,[16] Tab 1), but comparable to the best negolyte (cobaltocene,[17] Tab 1). As such, at 100% state-of-charge and utilizing the positive 2nd wave of complex **5** and 2nd negative wave of complex **2**, the initial cell voltage would be ~4V, almost 1V over the unsubstituted Ni(bpb). Although these particular complexes have insufficient solubility to be used in practical applications, several published methods to improve solubility could be utilized to offset this characteristic.[6,27] Additionally, the described approach can be applied to other redox carriers in the literature to enhance the cell potential for which they are a part.

Experimental

All syntheses were conducted under atmospheric conditions unless otherwise noted. The ligand H_2bpb was prepared according to literature procedure. All remaining reagents were purchased from commercial sources and used as received, including HATU ($C_{10}H_{15}F_6N_6OP$, CAS 148893-10-1). DMSO-d_6 was dried over activated molecular sieves before use. NMR spectra were obtained on a Bruker DRX 500 or Neo 500 spectrometer at room temperature, then processed and analyzed with MestReNova software (v11.0.4-18998). ^{1}H and ^{13}C chemical shifts are reported in parts per million (ppm) relative to TMS, with the residual solvent peak used as an internal reference. NMR multiplicities are reported as follows: singlet (s), doublet (d), triplet (t), quartet (q), multiplet (m), broad signal (br). Coupling constants (J) are reported in hertz (Hz). Infrared spectroscopy was performed on a Thermo Scientific Nicolet iS50 spectrometer using an ATR attachment (diamond crystal). All electrochemical analyses were carried out in an argon-filled glovebox or in an argon saturated solution. The supporting electrolyte, tetrabutylammonium hexafluorophosphate (Sigma, ≥98%), was recrystallized from absolute ethanol 3 times and evacuated prior to use. The DMF used for analysis was distilled over CaH_2 and stored over activated 3 Å molecular sieves prior to use. Cyclic voltammetry was performed with a Metrohm PGSTAT204 potentiostat in a three-electrode electrochemical electrochemical cell consisting of a glassy carbon disk working electrode (0.07 cm2, BASi), a Ag/Ag^+ reference electrode (BASi) containing 0.01 M $AgNO_3$ or $AgBF_4$ in MeCN, and a platinum wire counter electrode (23 cm, ALS). Drop cast technique was adapted from the literature.[28,29] All experiments were run at scan rates ranging from 20 to 300 mV/s in an MeCN (unless otherwise specified) electrolyte containing 1mM of the Ni complex and 0.1 M $TBAPF_6$. High resolution mass spectrometric data was obtained on a Waters Synapt G2, usingMassLynx software. Elemental analysis was performed at Los Alamos National Laboratory on the following instrument: CHNS-O Analyzer, Model No.: EA1112.

Synthesis of 4-(Dimethylamino)picolinic acid

The title compound was prepared from a modified literature procedure. 0.402 g (2.55 mmol) of 4-Chloro-2-pyridinecarboxylic acid and 4 ml of a 40 % by wt solution of dimethylamine in water was added to a Lab-Crest pressure reaction vessel (Andrews Glass Co.). The reaction was magnetically stirred and heated to 150 °C for 3 hr. After the reaction cooled to room temperature, the solvent was removed under vacuum yielding an off white solid. The solid was washed with 3 ml of EtOH and 5 ml of diethyl ether, collected on a fritted filter and dried, yielding the title compound (0.372 g, 72 % yield) as the HCl salt. ^{1}H NMR in D_2O was consistent with the literature. ^{1}H NMR (500 MHz, D_2O) δ 7.94 (d, J = 7.3 Hz, 1H), 7.19 (d, J = 2.7 Hz, 1H), 6.82 (dd, J = 7.2, 2.7 Hz, 1H), 3.20 (s, 6H).

Synthesis of H_2bpb-$(NMe_2)_2$

The proligand was prepared using standard HATU coupling conditions. In a 50 ml round bottom flask, which was dried in an oven at 150 °C overnight prior to use, was added 4-(dimethylamino)picolinic acid (0.277 g, 1.67 mmol), HATU (0.634 g, 1.67 mmol), and 5 ml of dry DMF. To the mixture, N,N-diisopropylethylamine (0.66 ml, 3.79 mmol) was added and the suspension was stirred at room temperature for 30 min. Next, o-phenylenediamine (0.081 g, 0.76 mmol) was added and the mixture was stirred at room temperature overnight. The DMF was then removed to yield a dark solid which was washed with DCM. The resulting off white material was dissolved in a 1:1 solution (10 ml) of 0.1 M aqueous KOH and DCM. This biphasic solution was stirred for 5 min then extracted with DCM (3 x 12 ml). The organic layer was dried and the solvent was removed. The solid was then purified on silica using a 10 % MeOH in DCM solution to elute the title compound (0.120 g, 40 % yield). ^{1}H NMR (500 MHz, $CDCl_3$) δ 10.33 (s, 2H), 8.15 (d, J = 5.8 Hz, 2H), 7.92 (dd, J = 5.9 Hz, 2H), 7.57 (d, J = 2.6 Hz, 2H), 7.26 (d, J = 9.5 Hz, 2H), 6.56 (dd, J = 3.1 Hz, 2H), 3.08 (s, 12H). ^{13}C NMR (126 MHz, $CDCl_3$) δ 164.08, 155.48, 150.18, 148.44, 130.43, 125.87, 124.48, 108.38, 105.56, 39.49.

Calculated for (M+Na): $C_{22}H_{24}N_6O_2Na$, 427.1859; found 427.1854. Calculated for (M+H): $C_{22}H_{25}N_6O_2$, 405.2039; found 405.2031 (found both ions)

Synthesis of [Ni(bpb-$(NMe_2)_2$)], 2

The proligand (0.120 g, 0.297 mmol) was suspended in MeCN (10 ml) and triethylamine was added (0.188 ml, 1.35 mmol) yielding a solution. Nickel(II) tetrafluoroborate hexahydrate (0.091 g, 0.270 mmol) was added to the solution, immediately forming an orange precipitate. This mixture was stirred at room temperature for 5 hours and the precipitate was collected on a fritted filter, washed with DCM (10 ml) and dried, yielding the desired nickel complex (0.118 g, 95 % yield) IR (ATR): 1604 (b s, C=O), 1564, 1544, 1525, 1474, 1451, 1434, 1383 (b s), 1273, 1070, 1028, 950, 936, 858, 794, 776, 767, 610, 573, 527, 468. HR-ESI-MS: m/z calculated for (M+Na) $C_{22}H_{22}N_6O_2NiNa$: 483.1055; found: 483.0999

Synthesis of H_2bpb-F

Preparation of the fluorinated proligand followed the same protocol for H_2bpb-$(NMe_2)_2$ with the only modification being the reaction was performed in an argon filled glovebox. 2-Picolinic acid (0.305 g, 2.48 mmol), HATU (0.942 g, 2.48 mmol), and DMF (5 ml) were added to a dry 50 ml round bottom flask equipped with a stir bar and N,N-diisopropylethylamine (0.981 ml, 5.63 mmol) was added. This solution was stirred at room temperature for 30 min. 4-fluoro-1,2-phenylenediamine (0.142 g, 1.13 mmol) was then added and the solution was stirred at room temperature for 24 hours. The majority of the solvent was then removed under reduced pressure leaving roughly 1 ml of the crude solution. Water was then added to precipitate the desired product which was collected on a fritted filter and dried (0.326 g, 86 % yield). ^{1}H NMR (500 MHz, $CDCl_3$) δ 10.40 (s, 1H), 10.01 (s, 1H), 8.60 (d, J = 4.3 Hz, 1H), 8.49 (d, J = 4.3 Hz, 1H), 8.30 (dd, J = 18.3, 7.8 Hz, 2H), 7.90 (dt, J = 16.0, 7.7 Hz, 3H), 7.74 – 7.61 (m, 1H), 7.55 – 7.47 (m, 1H), 7.48 – 7.39 (m, 1H), 6.97 (t, J = 9.5 Hz, 1H). ^{13}C NMR (126 MHz, CDCl3) δ 163.39, 162.79, 161.86, 159.91, 149.58, 148.38, 137.72, 132.97, 132.87, 126.82, 124.81, 122.72,

112.49, 112.31, 110.96, 110.74. Calculated for (M+Na): $C_{18}H_{13}FN_4O_2Na$, 359.0920; found 359.0922

Synthesis of [Ni(bpb-F], 3

Preparation of the complex was identical to the dimethylamine derivative. The proligand (0.091 g, 0.271 mmol) was suspended in MeCN (10 ml) and trimethylamine was added (0.075 ml, 0.541 mmol) yielding a solution. Nickel(II) tetrafluoroborate hexahydrate (0.084 g, 0.246 mmol) was added to the solution, immediately forming an orange precipitate. This mixture was stirred at room temperature for 5 hours and the precipitate was collected on a fritted filter, washed with DCM (10 ml) and dried, yielding the desired nickel complex (0.076 g, 79 % yield). 1H NMR (500 MHz, DMF-d_7) δ 8.66 – 8.53 (m, 2H), 8.29 (q, J = 7.4 Hz, 2H), 8.22 (dd, J = 8.8, 6.1 Hz, 1H), 7.82 (dd, J = 12.4, 7.7 Hz, 2H), 7.78 – 7.70 (m, 2H), 6.62 (dt, J = 10.2, 5.1 Hz, 1H). IR (ATR): 1652, 1632 (s, C=O), 1602, 1576, 1486, 1469, 1435, 1382, 1300, 1244, 1176, 1142, 1097, 1077, 1026, 996, 930, 889, 869, 796, 772, 676, 652, 621, 603, 552, 523, 487, 470, 450. HR-ESI-MS: m/z calculated for (M+Na) $C_{18}H_{11}FN_4O_2NiNa$: 415.0117; found 415.0074

Synthesis of H_2bpb-CF_3

2-Picolinic acid (0.215 g, 1.75 mmol), HATU (0.665 g, 1.75 mmol), and DMF (5 ml) were added to a dry 50 ml round bottom flask equipped with a stir bar and N,N-diisopropylethylamine (0.692 ml, 3.97 mmol) was added. This solution was stirred at room temperature for 30 min. 4-trifluoromethyl-o-phenylenediamine (0.140 g, 0.795 mmol) was then added and the solution was stirred at room temperature for 24 hours. Next, water was added to the solution and the crude product was extracted with DCM (2x20 ml). The organic fraction was washed again with water (10 ml) and dried with Na_2SO_4. The crude material was then purified on silica using 8 % MeOH in DCM to elute the desired product (0.169 g, 55 % yield). ^{1}H NMR (500 MHz, $CDCl_3$) δ 10.45 (s, 1H), 10.27 (s, 1H), 8.57 (dd, J = 21.6, 4.1 Hz, 2H),

8.33 (t, J = 8.0 Hz, 2H), 8.17 (d, J = 10.2 Hz, 2H), 7.93 (q, J = 7.8 Hz, 2H), 7.57 (d, J = 8.4 Hz, 1H), 7.54 – 7.42 (m, 2H). ^{13}C NMR (126 MHz, $CDCl_3$) δ 163.26, 163.05, 149.43, 149.32, 148.42, 148.40, 137.86, 137.82, 133.73, 129.78, 127.00, 126.94, 124.35, 123.36, 123.34, 122.85, 122.17, 122.14. Calculated for (M+Na): $C_{19}H_{13}F_3N_4O_2Na$, 409.0888; found 409.0878

Synthesis of [Ni(bpb-CF_3], 4

Preparation of the complex was identical to the dimethylamine derivative. The proligand (0.100 g, 0.259 mmol) was suspended in MeCN (10 ml) and trimethylamine was added (0.072 ml, 0.518 mmol) yielding a solution. Nickel(II) tetrafluoroborate hexahydrate (0.080 g, 0.235 mmol) was added to the solution, immediately forming an orange precipitate. This mixture was stirred at room temperature for 5 hours and the precipitate was collected on a fritted filter, washed with DCM (10 ml) and dried, yielding the desired nickel complex (0.091 g, 88 % yield). IR (ATR): 1648 (b s, C=O), 1607, 1589, 1562, 1526, 1497, 1472, 1437, 1382, 1314, 1259, 1238, 1141, 1094, 1056, 1026, 985, 886, 822, 802, 753, 680, 653, 642, 521, 451, 425. HR-ESI-MS: m/z calculated for (M+Na) $C_{19}H_{11}F_3N_4O_2NiNa$: 465.0085; found 465.0038.

Synthesis of H_2bpb-NO_2

2-Picolinic acid (0.155 g, 1.26 mmol), HATU (0.480 g, 1.26 mmol), and DMF (5 ml) were added to a dry 50 ml round bottom flask equipped with a stir bar and N,N-diisopropylethylamine (0.500 ml, 2.87 mmol) was added. This solution was stirred at room temperature for 30 min. 4-nitro-o-phenylenediamine (0.088 g, 0.575 mmol) was then added and the solution was stirred at room temperature for 24 hours. Next, water was added to the solution and the crude product was extracted with DCM (2x20 ml). The organic fraction was washed again with water (10 ml) and dried with Na_2SO_4. The crude material was then purified on silica using 10 % MeOH in DCM to elute the desired product (0.125 g, 60 % yield). Analytical data was identical to previously reported data.[30]

Synthesis of [Ni(bpb-NO_2], 5

H_2bpb-NO_2 (0.117g, 0.322 mmol) was placed in 8 ml of DMSO and triethylamine was added (0.204 ml, 1.46 mmol) yielding a yellow mixture. This mixture was heated to 100 °C and the mixture became a solution. Nickel(II) tetrafluoroborate hexahydrate (0.100 g, 0.293 mmol) was then added to the solution and an orange precipitate immediately formed. This mixture was stirred at 100 °C for an additional 3 hours. The precipitate was then collected on a fritted filter and washed with room temperature DMSO and DCM. The solid was then collected and dried yielding the desired product. IR (ATR): 3076, 1653 (b s, C=O), 1605, 1562, 1476, 1378, 1316, 1135, 1060, 994, 964, 892, 822, 803, 752, 731, 706, 680, 653, 616, 508, 467. EA: Calculated: %C 51.47, %H 2.64, %N 16.67, Found: %C 51.36, %H 2.53, %N16.23

Computational Details

Geometry optimizations of complexes **1-5** were performed in a gas phase by considering all possible spin multiplicities at particular charge state. Single-point energies in DMF and MeCN were obtained using self-consistent reaction field approach based on the integral equation formalism of the polarized continuum model (PCM).[31–33] All calculations were carried out with Gaussian 16 software package (Version B.01).[34] Frequency calculations were performed to ensure that the optimized structures represented minima on the potential energy surface for each species. Hybrid PBE0 functional was utilized since it was previously shown to produce the best correlation between calculated and experimental values of reduction potentials of Ni-coordination complexes.[22] For some of the complexes considered in this study in the 0 charge state, triplet spin (Ni^{2+}) states were found to be lower in energy by up to ~0.37 eV than the singlet spin (Ni^{2+}) state configurations (Tables S26, S27). Overstabilization of the high spin (HS) states as compared to the low spin (LS) configurations has been reported for hybrid functionals.[35–38] Based on the diamagnetic ^{1}H NMR spectra of the neutral charge state species **1-5** as well as the recent studies utilizing PBE0 functional for similar linked picolinamide Ni

complexes,[21] LS configurations are accepted as the ground electronic states and their energies are taken for the calculations of redox properties. Dispersion corrections (D3)[39] were applied to account for possible intramolecular noncovalent interactions that can be important for the correct description of solvent-complex interaction. As reported previously for various Ni-based catalysts,[40] PBE0-D3 was found to be the best functional in the complete benchmark set relative to estimated CCSD(T)/CBS reference data, with a mean absolute deviation from the reference values of 1.1 kcal/mol. LANL2DZ effective core potential (ECP) basis set[41] was employed for Ni, 6-311G(d)[42] basis set for C, N, O and 6-31G(d) for H atoms.[43]

The reduction potentials were computed using the revised Born-Haber cycle,[22] in which all reduction steps are referenced to a calculated absolute half-cell potential of a ferrocene couple, i.e., $Fc^0 + A^n \rightarrow Fc^+ + A^{n-1}$, as opposed to an experimental standard reference electrode, like the standard hydrogen electrode (SHE) or the saturated calomel electrode (SCE). Mulliken spin density analysis was applied to determine the oxidation states of the Ni center and nature of redox events (metal- or ligand-centered) at each charge transfer step. Mulliken spin densities of the studied complexes were found to have similar values in both environments (gas-phase or solvent) at each charge state.

Similar to the previous study on complex **1**[21] reporting a coordination of two MeCN molecules to the Ni center in the 2+/1+/0 charge states (Fig S3), two DMF molecules were considered in the $[Ni(bpb\text{-}R)]^{2+/1+/0}$ complexes in this study (Fig S4). In agreement with that, the Ni-solvent contacts are significantly longer ($R(Ni\text{-}O_{DMF})_{aver}$=2.60-3.36 Å) in the 0 charge state than in the 2+ charge state with direct Ni-O bonding ($R(Ni\text{-}O_{DMF})_{aver}$=2.10-2.12 Å). Migration of the two DMFs from the metal center in the 0 charge state results in the formation of hydrogen bonds in lieu of the Ni-O bonding, *i.e.* O_{DMF}-$H_{pyridine}$, H_{DMF}-O_{amide}, and H_{DMF}-N_{amide} (Fig S4). Hence, to avoid overestimating the impact of the hydrogen bonding interactions on the reduction potentials associated with the 1– and 2– charge states (Figs S5, S6), two DMF

molecules were considered in the 2+ and 1+ charge states as well as in 0 charge state as an intermediate one between the solvent-non-coordinating and the solvent-coordinating complexes exhibiting the Ni-O_{DMF} contacts.[21] For consistency, the same approach that was used for the calculations of the reduction potentials in **1** in MeCN[21] was employed for complexes **1-5** in DMF in this work.

Supporting Information

Supporting Information (solution state CV and DVP measurements of [Ni(bpb)]; DPV experiments of [Ni(bpb)] drop cast onto a glassy carbon disk electrode; geometrical parameters, Mulliken spin densities, spin states and Cartesian coordinates of the computed complexes by charge state; free energies in MeCN and DMF of the LS and HS state configurations of the $[Ni(bpb\text{-}R)(MeCN)_2]^0$ and $[Ni(bpb\text{-}R)(DMF)_2]^0$ complexes; free energies in MeCN and DMF of the $[Ni(bpb\text{-}R)(MeCN)_2]^{1+}$ and $[Ni(bpb\text{-}R)(DMF)_2]^{1+}$ complexes) is available from the Wiley Online Library or from the author.

Acknowledgements

This work was supported by the Laboratory Directed Research and Development (LDRD) program of Los Alamos National Laboratory under project number 20170046DR. I.A.P. acknowledges the support from J. Robert Oppenheimer Distinguished Postdoctoral Fellowship. C.R.F. would like to thank the Department of Energy's Summer Undergraduate Laboratory Internship program for funding. High resolution mass spectral data was acquired at the Center for Integrated Nanotechnologies, an Office of Science User Facility operated for the U.S. Department of Energy (DOE) Office of Science (agreement 2018BU0048). Los Alamos National Laboratory is operated by Triad, LLC, for the National Nuclear Security Administration of U.S. Department of Energy (Contract No. 89233218NCA000001).

Received: ((will be filled in by the editorial staff))
Revised: ((will be filled in by the editorial staff))
Published online: ((will be filled in by the editorial staff))

References

[1] G. L. Soloveichik, *Chem. Rev.* **2015**, *115*, 11533.
[2] R. W. Hogue, K. E. Toghill, *Curr. Opin. Electrochem.* **2019**, *18*, 37.
[3] R. Chen, D. Bresser, M. Saraf, P. Gerlach, A. Balducci, S. Kunz, D. Schröder, S. Passerini, J. Chen, *ChemSusChem* **2020**, 1.
[4] Y. Ding, C. Zhang, L. Zhang, Y. Zhou, G. Yu, *Chem. Soc. Rev.* **2018**, *47*, 69.
[5] Y. Ding, C. Zhang, L. Zhang, Y. Zhou, G. Yu, *Chem* **2019**, *5*, 1964.
[6] C. S. Sevov, S. L. Fisher, L. T. Thompson, M. S. Sanford, *J. Am. Chem. Soc.* **2016**, *138*, 15378.
[7] L. E. Vangelder, A. M. Kosswattaarachchi, P. L. Forrestel, T. R. Cook, E. M. Matson, *Chem. Sci.* **2018**, *9*, 1692.
[8] M. A. Goulet, L. Tong, D. A. Pollack, D. P. Tabor, S. A. Odom, A. Aspuru-Guzik, E. E. Kwan, R. G. Gordon, M. J. Aziz, *J. Am. Chem. Soc.* **2019**, 8.
[9] P. Huang, W. Ling, H. Sheng, Y. Zhou, X. Wu, X. X. Zeng, X. Wu, Y. G. Guo, *J. Mater. Chem. A* **2017**, *6*, 41.
[10] C. Zhang, Y. Qian, Y. Ding, L. Zhang, X. Guo, Y. Zhao, G. Yu, *Angew. Chem. Int. Ed.* **2019**, *58*, 7045.
[11] Y. Ding, C. Zhang, L. Zhang, H. Wei, Y. Li, G. Yu, *ACS Energy Lett.* **2018**, *3*, 2641.
[12] G.-M. Weng, B. Yang, C.-Y. Liu, G.-Y. Du, E. Y. Li, Y.-C. Lu, *Energy Environ. Sci.* **2019**, *12*, 2244.
[13] Y. Ding, Y. Li, G. Yu, *Chem* **2016**, *1*, 790.
[14] M. R. Gerhardt, L. Tong, R. Gómez-bombarelli, Q. Chen, M. P. Marshak, C. J. Galvin, A. Aspuru-guzik, R. G. Gordon, M. J. Aziz, *Adv. Energy Mater.* **2017**, 1601488.
[15] X. Wei, L. Cosimbescu, W. Xu, J. Z. Hu, M. Vijayakumar, J. Feng, M. Y. Hu, X. Deng, J. Xiao, J. Liu, V. Sprenkle, W. Wang, *Adv. Energy Mater.* **2015**, *5*, 1.
[16] Y. Yan, S. G. Robinson, M. S. Sigman, M. S. Sanford, *J. Am. Chem. Soc.* **2019**, *141*, 15301.
[17] Y. Ding, Y. Zhao, Y. Li, J. B. Goodenough, G. Yu, *Energy Environ. Sci.* **2017**, *10*, 491.
[18] B. E. Schurr, O. Nachtigall, L. E. Vangelder, J. Drappeau, W. W. Brennessel, E. M. Matson, B. E. Schurr, O. Nachtigall, L. E. Vangelder, J. Drappeau, *J. Coord. Chem.* **2019**, *72*, 1267.
[19] L. E. VanGelder, E. M. Matson, *J. Mater. Chem. A* **2018**, *6*, 13874.
[20] R. M. Darling, K. G. Gallagher, J. A. Kowalski, S. Ha, F. R. Brushett, *Energy Environ. Sci.* **2014**, *7*, 3459.
[21] T. Chu, I. A. Popov, G. A. Andrade, S. Maurya, P. Yang, E. R. Batista, B. L. Scott, R. Mukundan, B. L. Davis, *ChemSusChem* **2019**, *12*, 1304.
[22] L. E. Roy, E. Jakubikova, M. G. Guthrie, E. R. Batista, *J. Phys. Chem. A* **2009**, *113*, 6745.
[23] D. J. Barnes, R. L. Chapman, R. S. Vagg, E. C. Watton, *J. Chem. Eng. Data* **1978**, *23*, 349.
[24] I. A. Popov, N. Mehio, T. Chu, B. L. Davis, R. Mukundan, P. Yang, E. R. Batista, *ACS Omega* **2018**, *3*, 14766.
[25] I. A. Popov, B. L. Davis, R. Mukundan, E. R. Batista, P. Yang, *Front. Phys.* **2019**, *6*, 1.
[26] S. K. Dutta, U. Beckmann, E. Bill, T. Weyhermuller, K. Wieghardt, *Inorg. Chem.* **2000**, *39*, 3355.
[27] J. A. Suttil, J. F. Kucharyson, I. L. Escalante-Garcia, P. J. Cabrera, B. R. James, R. F. Savinell, M. S. Sanford, L. T. Thompson, *J. Mater. Chem. A* **2015**, *3*, 7929.

[28] A. Choi, H. Jeong, S. Kim, S. Jo, S. Jeon, *Electrochim. Acta* **2008**, *53*, 2579.
[29] R. McGuire, D. K. Dogutan, T. S. Teets, J. Suntivich, Y. Shao-Horn, D. G. Nocera, *Chem. Sci.* **2010**, *1*, 411.
[30] A. F. Abdel-Magied, W. A. A. Arafa, T. M. Laine, A. Shatskiy, M. D. Kärkäs, B. Åkermark, E. V. Johnston, *ChemCatChem* **2017**, *9*, 1583.
[31] E. Cancès, *J. Chem. Phys.* **1997**, *107*, 3032.
[32] B. Mennucci, E. Cancès, J. Tomasi, *J. Phys. Chem.* **1997**, *101*, 10506.
[33] E. Cancès, B. Mennucci, *J. Math. Chem.* **1998**, *23*, 309.
[34] M. J. Frisch, E. Al, *Gaussian 16 (Revision B.01)*, Gaussian, Inc., Wallingford CT, **2016**.
[35] J. N. Harvey, *Principles and Applications of Density Functional Theory in Inorganic Chemistry I*, Springer, Berlin, **2004**.
[36] M. Swart, *Int. J. Quantum Chem* **2013**, *113*, 2.
[37] M. Reiher, O. Salomon, B. A. Hess, *Theor. Chem. Acc.* **2001**, *107*, 48.
[38] B. Pinter, A. Chankisjijev, P. Geerlings, J. N. Harvey, F. D. Proft, *Chem. Eur. J.* **2018**, *24*, 5281.
[39] S. Grimme, J. Antony, S. Ehrlich, H. Krieg, *J. Chem. Phys.* **2010**, *132*, 154104.
[40] M. Steinmetz, S. Grimme, *ChemistryOpen* **2013**, *2*, 115.
[41] P. J. Hay, W. R. Wadt, *J. Chem. Phys.* **1985**, *82*, 270.
[42] A. D. McLean, G. S. Chandler, *J. Chem. Phys.* **1980**, *72*, 5639.
[43] P. C. Hariharan, J. A. Pople, *Theor. Chim. Acta* **1973**, *28*, 213.